H1 Results in Deep Inelastic Scattering

Gregorio Bernardi

H1 Collaboration
LPNHE – Université de Paris 6-7, CNRS-IN2P3
e-mail: gregorio@mail.desy.de

Abstract. Recent deep inelastic results from the H1 collaboration are presented. The topics covered include inclusive diffractive physics, the determination of α_S using the event shapes, the study of the hadronic final state at low x with single particles and with jets, the structure function measurements in particular F_2^p at low Q^2 and the high Q^2 physics both in neutral and charged current.

I INTRODUCTION

The first two years after the commissionning of the first ep collider HERA in May 1992 were devoted in deep inelastic scattering (DIS) to the observation of the new processes which would become the main subject of study nowadays in DESY: The observation of the rise of the F_2^p proton structure function at low x [1,2] was the first of this type of measurement which is still progressing in terms of precision and possibilities of QCD test, α_S and gluon density determination. The rich phenomenology at low x could also be studied in the measurement of hadronic final state properties. The clear observation of diffractive events [3,4] paved the way to a detailed and not yet finished study of one of the most obscure problem of the strong interaction. The observation of high Q^2 charged and neutral current [5,6] with very low statistics at that time, but in a perfect experimental environment allowed a glimpse to what will be the future of the HERA collider. The following years (1994,1995,1996) are the one covered in this report. They allowed the first precise measurements of the phenomena mentionned above, besides many others. In 1995, the H1 collaboration upgraded the backward detectors of the experiment, introducing in particular a more precise drift chamber (BDC) to measure the polar angle of the scattered electron, and a new SPACAL calorimeter with better hadronic containment, better granularity and better angular acceptance. The results obtained have fullfilled the expectations and a new step in precision could thus be reached for the low Q^2 physics.

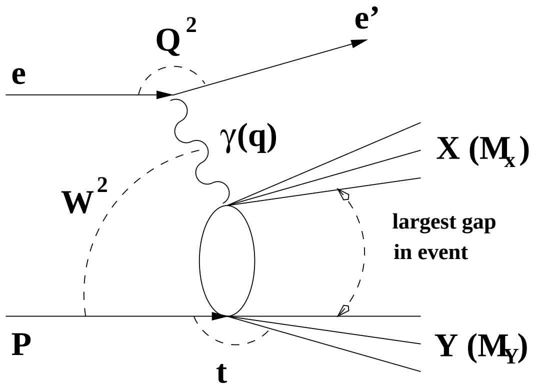

FIGURE 1:

Inclusive Variables

$Q^2 = -q^2$

$x = Q^2/(2\ q \cdot P)$

$y = (q \cdot P)/(e \cdot P)$

$W = Q^2\ (1-x)/x \simeq ys$

$M = \sqrt{sx} = \sqrt{Q^2/y}$

Diffractive Variables

$x = \beta \cdot x_{I\!P}$

$\beta\ =\ Q^2/(2\ q \cdot (P-Y))\ \ \simeq\ \frac{Q^2}{Q^2+M_X^2}$

$x_{I\!P}\ =\ q \cdot (P-Y)/(q \cdot P)\ \simeq\ \frac{Q^2+M_X^2}{Q^2+W^2}$

$t = (P-Y)^2$

In the following we will often refer to the inclusive and diffractive kinematic variables, and to their method of reconstruction so let us introduce them here, using fig. 1 as an illustration of the basic DIS process. The exchanged boson is a photon in most of the cases, but the exchange of Z° and $W^\pm$ becomes sizeable at high Q^2. The basic DIS selection requires the detection of an electromagnetic cluster representing the scattered electron[1] above a certain energy threshold which is typically around 10 GeV, and the presence of a reconstructed interaction vertex in order to reject the beam associated background and to improve the reconstruction quality. Further requirements are applied depending on the analyses as we will see later. The hadronic final state is resolved in two systems X and Y in the study of diffraction using a specific selection.

The kinematics can be reconstructed at HERA with different methods for the neutral current (NC) events (electron only (e), Σ, Double Angle (DA)), but only one (hadrons only, h) for the charged current (CC) since then only the hadronic final state is measured. In general H1 uses for the NC the e and the Σ method, since they complete each other. The h method is used for the CC analysis, while the DA has been used as a cross-check in the high Q^2 NC analysis.

Section II discusses the diffractive physics results, section III the determination of α_S using the event shapes, section IV the study of the hadronic final state at low x with single particles and with jets, section V the structure function measurements and section VI the high Q^2 NC and CC physics.

---

[1] HERA can run both with e^+ and e^-, but here "electron" is used both for e^+ and e^-.

II INCLUSIVE DIFFRACTION

The DIS diffractive events are characterized by a hadronic final state having a large gap in rapidity (see fig. 1) between the system X which is associated to the interacting parton and the system Y which is related to the fragments of the proton. The interaction can be described by the exchange of a colourless object (a "pomeron", $I\!P$) which creates the gap observed between the two systems. Experimentally these DIS events are selected by the absence of hadrons in the pseudorapidity interval $3.4 < \eta < 7.5$. The system X (Y) is composed of all particles produced backward[2] (forward) of this gap. The limit $\eta = 7.5$ for the system Y restricts its mass to $M_Y < 1.6$ GeV and its squared momentum to $|t| < 1.0$ GeV^2. Hard diffraction can be quantified by the measurement of the diffractive structure function $F_2^{D(3)}$ which is related to the triple differential cross-section of diffractive events via:

$$\frac{\mathrm{d}^3\sigma^D_{ep\to e'XY}}{\mathrm{d}\beta \mathrm{d}Q^2 \mathrm{d}x_{I\!P}} = \frac{4\pi\alpha^2}{\beta Q^4}(1-y+\frac{y^2}{2}) \cdot F_2^{D(3)}(Q^2,\beta,x_{I\!P})$$

The kinematic range of the 1994 measurement is $2.5 < Q^2 < 65\,\mathrm{GeV}^2$, $0.01 < \beta < 0.9$ and $0.0001 < x_{I\!P} < 0.05$. This analysis was already reported by H1 [7], but the interpretation of the measurement has progressed since that first observation of the "factorization breaking". This "breaking" means that in $F_2^{D(3)}$ a pomeron flux of the type $x_{I\!P}^{-n}$ cannot be factorized out, unless n is taken as a function of Q^2 and β. H1 has already shown with the 1994 data that n depends on β but not on Q^2 [8]. In fig. 2 is shown the quantity $x_{I\!P} \cdot F_2^{D(3)}(Q^2,\beta,x_{I\!P})$ as a function of $x_{I\!P}$ for different values of β and Q^2. The deviations from factorization are clearly visible and a possible explanation is the contribution from so-called sub-leading trajectories to the measured cross-sections which may be identified with the exchange of particles carrying the quantum numbers of the physical meson states. After the pomeron, the next-leading exchanges are the trajectories of the f_2, ρ, ω and a_2 mesons, which are expected to give a contribution to $x_{I\!P} \cdot F_2^{D(3)}(Q^2,\beta,x_{I\!P})$ which rises with x. In fig. 2 is also shown the result of a fit to the data in which both a pomeron component of the type $\mathrm{A}(\beta,Q^2)\cdot x_{I\!P}^{-n_{I\!P}}$ and a meson component $C_M \cdot F_2^M(\beta,Q^2)\cdot x_{I\!P}^{-n_M}$ contribute to $F_2^{D(3)}$ (see [8] for details) The parameters C_M, $n_{I\!P}$ and n_M are free parameters in the fit together with $A(\beta,Q^2)$ at each value of β and Q^2. The function $F_2^M(\beta,Q^2)$ is taken from the GRV parametrization of the pion structure function [9]. The result of the fit assuming a maximal interference between the pomeron and meson amplitudes is shown in the upper curve of each bin of fig. 2, and has a $\chi^2/ndf = 165/156$. The lower line represent the pomeron contribution alone, while the middle one represent the sum of the two contribution without taking into account the interfence. The influence of

[2] The positive z axis is defined at HERA as the incident proton beam direction.

the meson exchange is limited at relatively high $x_{\mathbb{P}}$ (> 0.05) and is stronger at low β. After correcting for the integration over t, the resulting pomeron and meson intercepts are

$$\alpha_{x_{\mathbb{P}}}(0) = 1.18 \pm 0.02(\mathrm{stat}) \pm 0.04(\mathrm{syst}) \quad ; \quad \alpha_M(0) = 0.6 \pm 0.1(\mathrm{stat}) \pm 0.3(\mathrm{syst})$$

While the value of α_M is consistent with that expected for the exchange of the mesons previously cited, the value of $\alpha_{x_{\mathbb{P}}}(0)$ is somewhat higher than the one obtained when parametrizing the total cross-section of soft hadronic interaction [10].

A QCD analysis [11] of $\tilde{F}_2^D(\beta, Q^2)$ which is obtained by integrating $F_2^{D(3)}(Q^2, \beta, x_{\mathbb{P}})$ between $0.0003 < x_{\mathbb{P}} < 0.05$ reveals the partonic structure of the pomeron (mesonic effects are here neglected, but have been checked not to change the interpretation). It is found to be dominated by a hard gluon density peaking at $x_{g/\mathbb{P}} \simeq 1$, and about 80% of its momentum is carried by gluons at Q^2 below 65 GeV^2 . This results is confirmed by the analysis of the hadronic final state of DIS diffractive events [12].

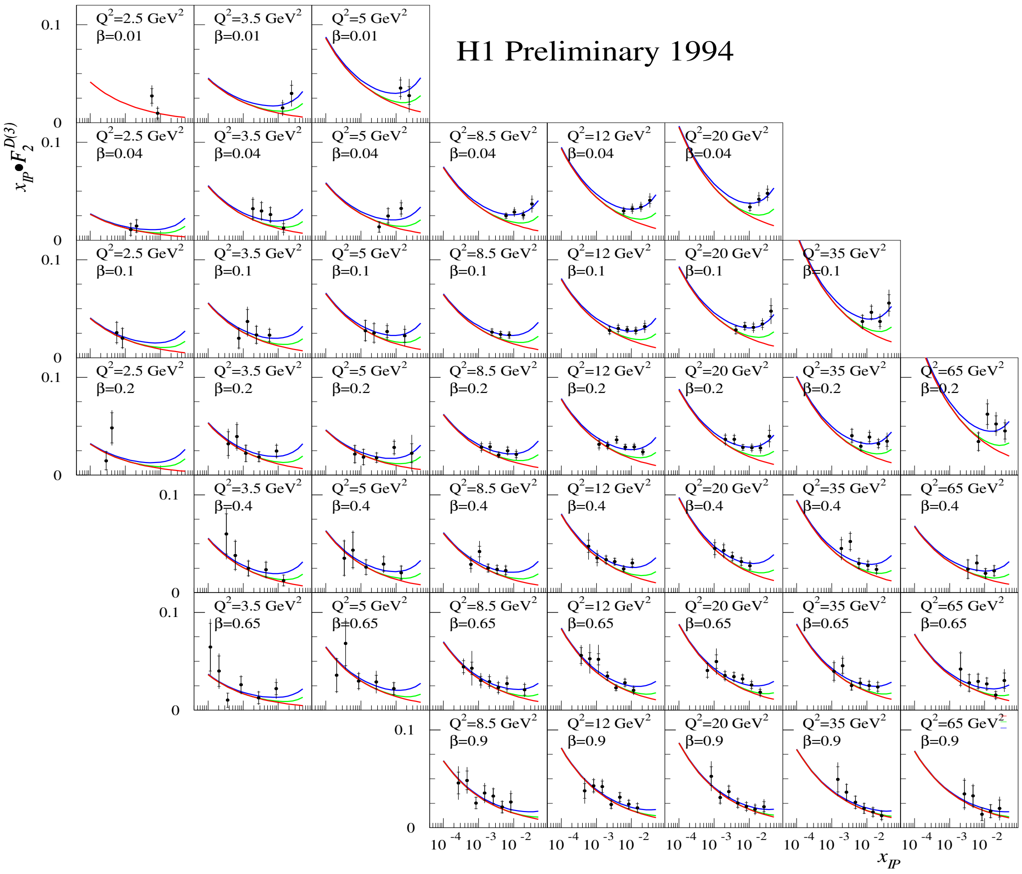

FIGURE 2. *$x_{\mathbb{P}} \cdot F_2^{D(3)}(Q^2, \beta, x_{\mathbb{P}})$ as a function of $x_{\mathbb{P}}$ for different values of β and Q^2. Also shown is the phenomenological fit described in the text.*

Diffractive DIS with a Leading Proton in the Forward Proton Spectrometer (FPS)

In 1995 the FPS has been installed in H1 allowing leading protons with energies between 500 and 760 GeV and scattering angles below 1 mrad to be detected. Its main use is, after detection a leading proton, to measure the variable $\xi = 1 - E'_p/E_p$, where E_p and E'_p are the proton energy before and after the interaction. ξ is defined as $x_{I\!P}$ in terms of 4-vectors and may be interpreted as the fraction $x_{\pi/p}$ of the proton's 4-momentum carried by the exchanged object. It is thus possible to define a Leading Proton structure function $F_2^{LP(3)}$ in the same way as $F_2^{D(3)}$, but in which β is interpreted as the fraction $x_{q/\pi}$ of the momentum of the particle π carried by the struck quark. The structure function $F_2^{LP(3)}$ shown in fig. 3 has been measured for events with a proton of $p_\perp < 200\,\mathrm{MeV}$ and $E'_p = 580 - 740\,\mathrm{GeV}$ using the data collected in 1995 which represent an integrated luminosity of 1.44 pb^{-1} [13].

The measurement shows a weak ξ dependence as expected for pion exchange and a logarithmic rise with Q^2. Although the behaviour is reproduced in shape by a pion-exchange model introduced in RAPGAP [14] (GRV-LO pion parton densities are used), the overall normalization of the simulation is too low by about a factor of two. The factorization of $F_2^{LP(3)}$ as $f_{\pi/p}(\xi) \cdot F_2^{\pi}(\beta, Q^2)$ could not be established yet, although the data are not incompatible with this hypothesis. The upgraded FPS and the additional data taken in 1996 should allow to answer this questions in the near future.

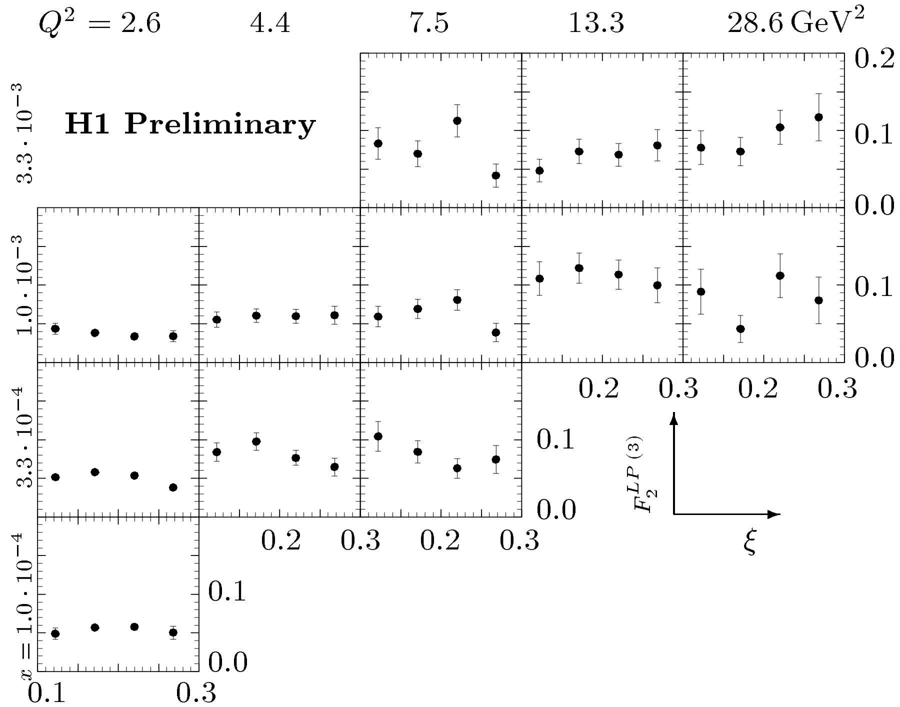

FIGURE 3. *Measurements of $F_2^{LP(3)}$ as a function of ξ in bins of x and Q^2.*

III α_S FROM THE DIS EVENT SHAPES

At HERA, in the Breit frame[3] the DIS event shapes can be studied in the "current" hemisphere in a similar way than in one of the two hemispheres measured at LEP [15]. The scale correponding to $\sqrt{s}/2$ in e^+e^- collisions is $Q/2$, i.e. at HERA it is possible to vary continuously this scale and study the evolution of the observables as a function of Q. The event shapes variables which have been studied are the thrust T_c and T_z i.e. respectively defined along the thrust axis ($\mathbf{n_T}$) or along the hemisphere axis ($\mathbf{n}$), the jet mass ρ_c or the jet broadening (B_c). We refer to [16] for a discussion of B_c and concentrate here on the first 3 variables which are defined as

$$T_c = \max \frac{\sum_h |\, \mathbf{p}_h \cdot \mathbf{n}_T \,|}{\sum_h |\, \mathbf{p}_h \,|} \quad T_z = \frac{\sum_h |\, \mathbf{p}_h \cdot \mathbf{n} \,|}{\sum_h |\, \mathbf{p}_h \,|} \quad \rho_c = \frac{M^2}{Q^2} = \frac{(\sum_h p_h)^2}{Q^2}$$

The sums extend over all hadrons h with 4-momentum $p_h = [E_h, \mathbf{p}_h]$ fullfilling $\cos(\mathbf{p}_h \cdot \mathbf{n}) > 0$, and the current hemisphere axis coincides with the exchanged boson direction. The study has been made for 8 GeV $< Q <$ 68 GeV using 2.9 pb^{-1} of 1994 data at low Q^2 and 10.9 pb^{-1} in the 1994-1996 data at high Q^2.

The normalized differential spectrum of the T_c variable and its mean value as a function of Q are shown as an example in fig 4. The mean value exhibit a strong Q dependence, decreasing with rising Q^2, i.e. the energy flow in the current hemisphere becomes more collimated. The data are well described by the LEPTO Monte Carlo model [18] for all Q. This distribution is in gross agreement with the e^+e^- data. The differences can be understood as due to the different analysis methods used at HERA and LEP, and to the different physics effects related to the nature of the interaction involved.

The QCD analysis of these distributions is built upon the fact that the mean value of any "infrared safe" event shape variable F such as $1 - T_c, (1 - T_z)/2$ or ρ_c can be decomposed in DIS and in e^+e^- annihilation as [17]

$$\langle F \rangle = \langle F \rangle^{\mathrm{pert}} + \langle F \rangle^{\mathrm{pow}}$$

with the perturbative part and the power correction part given by

$$\langle F \rangle^{\mathrm{pert}} = c_1\, \alpha_s(Q) + c_2\, \alpha_s^2(\mu_R)$$
$$\langle F \rangle^{\mathrm{pow}} = a_F\, \frac{16}{3\,\pi}\, \frac{\mu_I}{Q}\, \ln^p \frac{Q}{\mu_I} \left[\bar{\alpha}_0(\mu_I) - \alpha_s(Q) - \frac{\beta_0}{2\,\pi} \left(\ln \frac{Q}{\mu_I} + \frac{K}{\beta_0} + 1 \right) \alpha_s^2(Q) \right]$$

The coefficients $c_1,\ c_2$ are obtained from $\mathcal{O}(\alpha_s^2)$ DISENT calculations [19]. The power (or hadronization) corrections are believed to stem from a universal soft gluon phenomenon associated with the behaviour of the running coupling at small momentum scales, i.e. the usual $1/Q$ corrections are not necessarily

---

3) Defined such as the exchanged boson is purely space-like with 4-momentum (0,0,0,-Q).

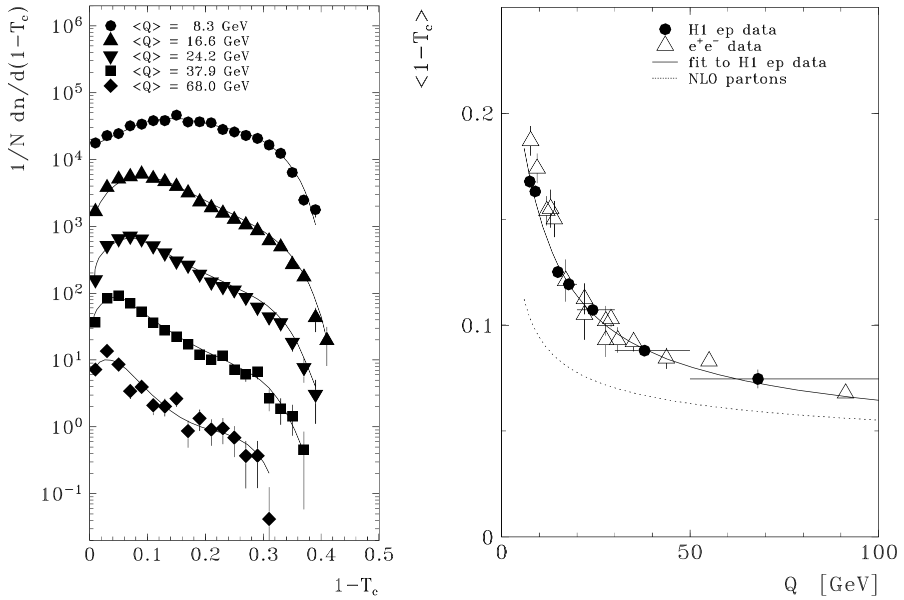

FIGURE 4. *a) Distributions of 1-T_c in bins of Q^2. b) Comparison of the evolution of the mean of 1−T_c as a function of Q in DIS and e^+e^-.*

related to hadronisation. The universality means that the phenomenon could be described by calculable coefficients a_F and p which are process dependent together with a few non-perturbative parameters like $\bar{\alpha}_0(\mu_I)$ which has to be evaluated at some 'infrared matching' scale $\Lambda \ll \mu_I \ll Q$. The values of the means at the different Q^2 values can thus be fitted to give a simultaneous determination of $\bar{\alpha}_0(\mu_I)$ and of the strong coupling constant $\alpha_S(M_Z)$ independently of any fragmentation model. The results are given below for ep data, followed by the parameters obtained in e^+e^- data for comparison.

Observable	$\bar{\alpha}_0(\mu_I = 2$ GeV)	$\alpha_s(M_Z)$	χ^2/ndf
$\langle 1 - T_c \rangle$	$0.497 \pm 0.005\ ^{+0.070}_{-0.036}$	$0.123 \pm 0.002\ ^{+0.007}_{-0.005}$	5.0/5
$\langle 1 - T_z \rangle / 2$	$0.507 \pm 0.008\ ^{+0.109}_{-0.051}$	$0.115 \pm 0.002\ ^{+0.007}_{-0.005}$	8.5/5
$\langle \rho_c \rangle$	$0.519 \pm 0.009\ ^{+0.025}_{-0.020}$	$0.130 \pm 0.003\ ^{+0.007}_{-0.005}$	3.1/5
common fit	$\mathbf{0.491 \pm 0.003\ ^{+0.079}_{-0.042}}$	$\mathbf{0.118 \pm 0.001\ ^{+0.007}_{-0.006}}$	39/19
$\langle 1 - T_{ee} \rangle$	$0.519 \pm 0.009\ ^{+0.093}_{-0.039}$	$0.123 \pm 0.001\ ^{+0.007}_{-0.004}$	10.9/14
$\langle M_H^2/s \rangle$	$0.580 \pm 0.015\ ^{+0.130}_{-0.053}$	$0.119 \pm 0.001\ ^{+0.004}_{-0.003}$	10.9/14

The event shapes are compatible with a universal power correction parameter $\bar{\alpha}_0 \approx 0.5$ within $\pm 20\,\%$ which is also valid at LEP. The $\alpha_s(M_Z)$ determination has the same precision than the one obtained from a large set of event shape analyses in e^+e^- at the Z resonnance [20], and the error is here dominated by theoretical uncertainties due to as yet unknown higher order QCD corrections.

IV BFKL EFFECTS ON HADRONIC FINAL STATE

At HERA the hadronic final state is measured in a precise way, and renders possible a test of the QCD dynamics at high p_T. The analyses described below are performed at Q^2 between 5 and 100 GeV^2 and between 10^{-4} and 10^{-2} in x. The measured distributions are corrected for detector effects to the hadron level, and compared to $\mathcal{O}(\alpha_s^2)$ next to leading order (NLO) calculations or to models based on QCD phenomenology, see fig. 5. For the dijet production rate these NLO calculations are available and implemented in the DISENT [19] and MEPJET [21] Monte Carlo programs.

Another approach is to perform a resummation of the leading logarithms of the DGLAP [22] type ($(\alpha_s \ln \frac{Q^2}{Q_0^2})^n$ terms) or of the BFKL [23] type $(\alpha_s \ln \frac{1}{x})^n$ terms) the latter being expected to dominate at low x. The DGLAP approach is used in the LEPTO [18] and HERWIG [24] event generators in which leading log partons showers are added to leading order matrix elements (MEPS) in combination with a string or cluster hadron fragmentation model. The BFKL resummation is not yet available in event generators, but since there is no k_t ordering in this approach, contrarily to the DGLAP one, and since this characteristic is also present in the colour dipole model (CDM) as implemented in the ARIADNE [25] event generator, it is possible to have first clues on the underlying dynamics by confronting the data to ARIADNE.

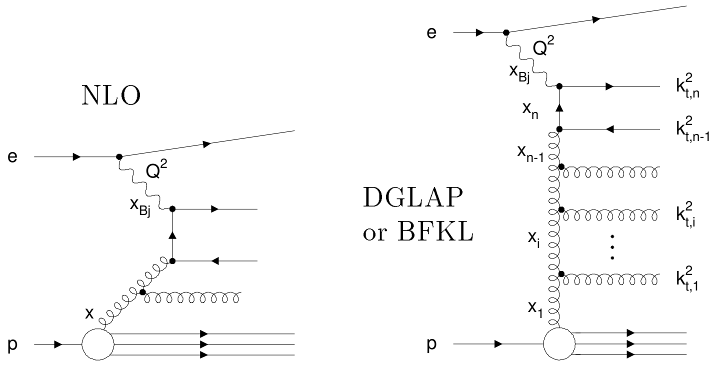

FIGURE 5. *a) Schematic representation of DIS in NLO and b) in a parton cascade model of the DGLAP or BFKL type.*

To measure the dijet rate, events with two jets having a cone radius of one and a transverse energy $E_T > 5$ GeV are selected if the difference in the hadronic center of mass (h.c.m.) $\Delta\eta^*_{max} < 2$. The dijet rate, given by the ratio of two-jets events to the total number of DIS events in the same kinematical region, is presented in fig. 6a,b as a function of Q^2 and x and compared to the QCD models and calculations predictions. The description of the data by ARIADNE is excellent but this cannot be interpreted yet as a proof for a BFKL effect since, surprizingly, LEPTO fails to describe the data even at high

Q^2 and moderate x, a fact which cannot be attributed to the hadronization correction since they are relatively small ($< 25\%$) as can be verified by the good agreement between DISENT and LEPTO.

Recently a sensitive test of BFKL evolution based on the transverse momentum spectra of single particles has been proposed [26]. The hard tail of the p_T spectrum was shown to originate from parton radiation while hadronization effects were suppressed. Since parton emissions in the central region of the h.c.m. are less restricted for a k_T unordered scenario, a harder p_T spectrum than those expected in DGLAP models could be a BFKL signature.

The measured charged particle spectra [27] (for 0.5$< \eta^* < 1.5$) are shown in fig. 6c. While at large values of x and Q^2 all models describe the data well, the DGLAP based models fail to describe the high p_T tail at small x. ARIADNE gives a good description of the data over the full kinematic range, hinting that the first BFKL effects could be in sight.

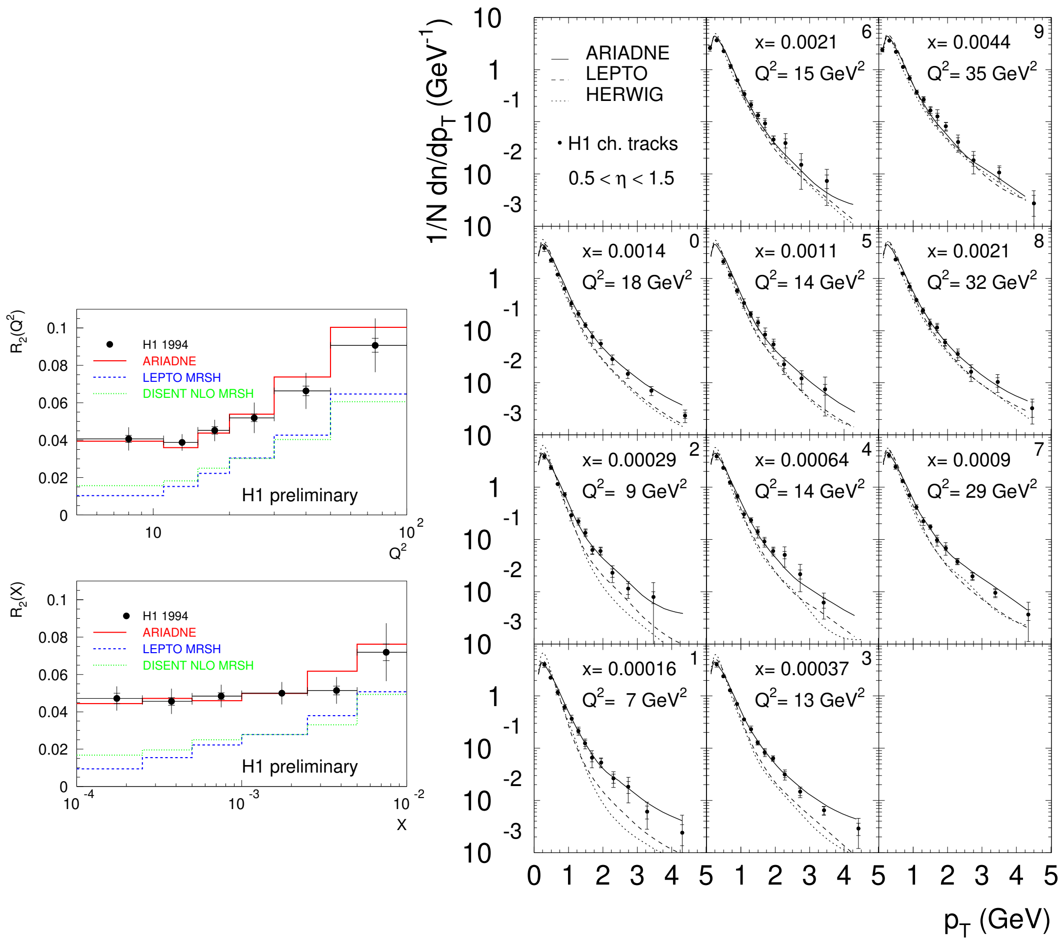

FIGURE 6. *Dijet rate as a function of Q^2 (a) and x (b). c) Distribution of the transverse momentum of central charged tracks in bins of Q^2 and x.*

V STRUCTURE FUNCTIONS

One of the major physics issues at HERA is the measurement of the proton structure functions $F_2^p(x,Q^2)$, $F_L^p(x,Q^2)$ and $xF_3^p(x,Q^2)$, this last one being not measured yet at HERA due to lack of statistics. The rise of F_2 with decreasing x has already been established from the first measurements with the data taken in 1992 and 1993 [1,2,28,29]. Since then, impressive progress has been made, both in the extension of the kinematic range of the F_2 measurement as illustrated in fig. 7a, and in the precision achieved.

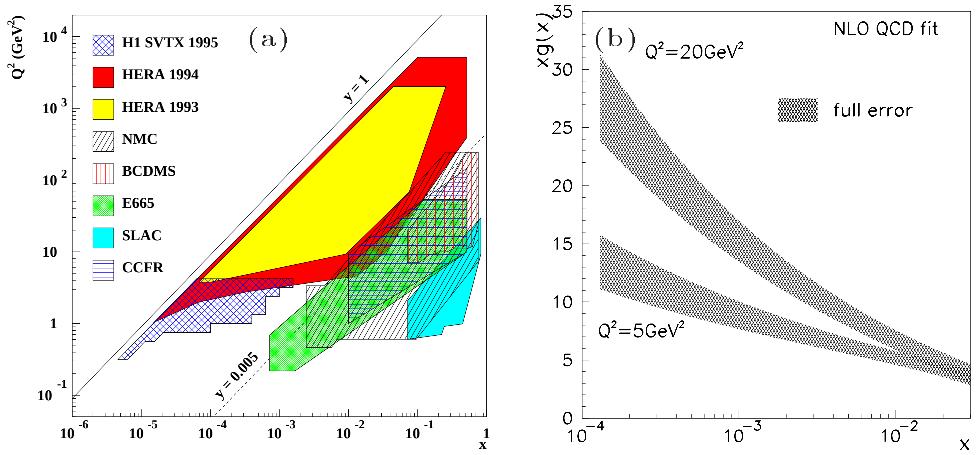

FIGURE 7. *a) The kinematic region of various structure function measurements. b) The gluon density at $Q^2 = 5$ and 20 GeV^2 extracted by H1 NLO-DGLAP fit.*

With a luminosity of about 2 pb^{-1} accumulated in the 94 running period $F_2^p(x,Q^2)$ has been measured by H1 [30,31] between $1.5 - 5000$ GeV^2 in Q^2 and $0.78 - 0.01$ in y, reaching at low y the kinematic region of the fixed target experiments. In the high statistic region an error of about 5% was achieved, allowing precise QCD tests. A NLO-DGLAP fit was performed on this data (restricted to $Q^2 > 5$ GeV^2) together with BCDMS [32] and NMC [33] data, giving a good description of F_2 over the whole kinematic range, surprisingly even at the lowest Q^2 of 1.5 GeV^2. From the fit, the gluon density was extracted (fig. 7b), showing a sharp rise at low x.

More recently two further topics have been adressed by H1 in this field and will be detailed in the following: i) a dedicated analysis of the very high y region (up to $y = 0.78$) of the 94 data used in conjunction with a NLO QCD fit to the low y part of the data, allowed the longitudinal structure function F_L to be determined for the first time at HERA [34], giving a consistent picture within the QCD framework; ii) the analysis of 0.11pb^{-1} data taken in 95 after the upgrade of the backward region of the H1 detector and with a shifted interaction vertex, therefore increasing the acceptance at low Q^2 and low x. This allowed F_2 to be measured down to Q^2 of 0.35 GeV^2 [35], and the transition between perturbative and non-perturbative QCD to be reached.

A The Longitudinal Structure Function

In the single photon exchange approximation the relation between the differential cross-section, the structure function F_2 and the longitudinal structure function F_L can be expressed as

$$\frac{d^2\sigma}{dxdQ^2} = \frac{2\pi\alpha^2}{xQ^4}\left[(2(1-y)+y^2)F_2(x,Q^2) - y^2F_L(x,Q^2)\right]$$

where F_L is related to the cross-section of transverse and the longitudinal polarised photons, σ_T and σ_L: $F_L = F_2 - 2xF_1, R = \sigma_L/\sigma_T = F_L/F_2 - F_L$. Note that the influence of F_L to the DIS cross-section is most important in the high y region.

The conventional method to measure F_L consists in unfolding the DIS cross-section measured at different center of mass energies as made by various fixed target experiments [36,37]. The H1 collaboration has published a determination of F_L at 8.5 GeV$^2 < Q^2 <$ 35 GeV^2 and at very small x values between $1.3 \cdot 10^{-4}$ and $5.5 \cdot 10^{-4}$, using the so called "subtraction method" [34]: as the behaviour of F_2 can be described with a good precision by a NLO DGLAP fit over several orders of magnitude in Q^2, such a fit is performed on the F_2 data at $y \leq 0.35$, where the influence of F_L is negligible. After an extrapolation up to $y = 0.78$ this contribution of F_2 to the cross-section is subtracted and the difference attributed to F_L. The results of this procedure is displayed in fig. 8 for six points in x and Q^2.

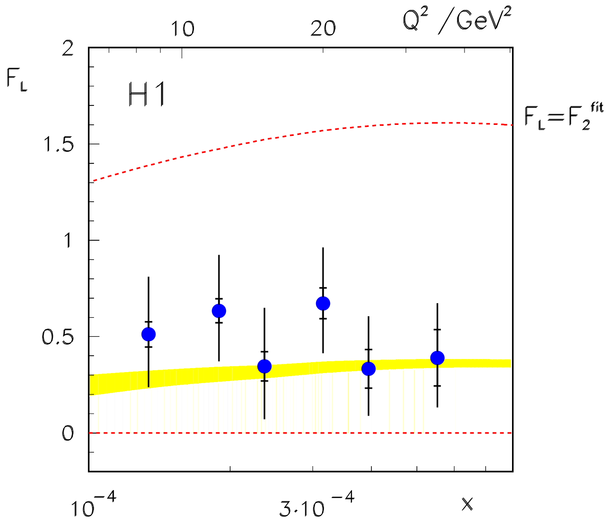

FIGURE 8. *The longitudinal structure function F_L at different values of x and Q^2*

The F_L obtained excludes the extreme limits of $F_L = 0$ and $F_L = F_2$ by 2.3 and 4.0 times the total error on F_L and is consistent with the Altarelli-Martinelli prediction [38] obtained in perturbative QCD (pQCD) shown as the band in fig. 8.

B F_2^p at low x and low Q^2

In the region of pQCD ($Q^2 \geq 1$ GeV^2), the evolution of F_2 is nicely described by the model of Glück, Reya, Vogt (GRV) [39], which evolves valence like parton distribution at a low starting scale of 0.34 GeV^2 according to NLO DGLAP equations. At $Q^2 \simeq 0$, in the photoproduction region, the measured cross-sections are in agreement with the Donnachie-Landshoff model (DOLA) [41], which assumes a Q^2-independent Regge behaviour up to a few GeV^2, due to the exchange of a "soft" pomeron.

The recently published F_2 measurements at low Q^2 [35] are shown in fig. 9. They give new experimental information for the transition region between the perturbative and non-perturbative QCD at 0.35 GeV^2 $< Q^2 <$ 3.5 GeV^2 and for x values down to $6 \cdot 10^{-6}$, and are compared to previous measurements done in "fixed target" mode and to various phenomenological models.

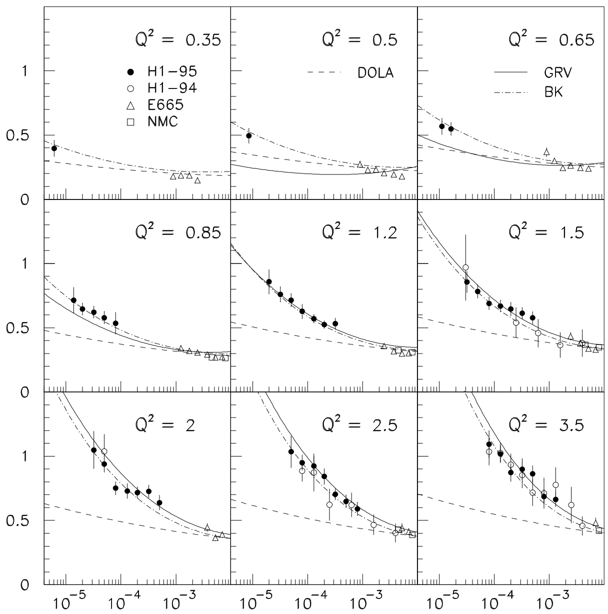

FIGURE 9. *The F_2 structure function measurement at low Q^2 and low x compared to fixed targed data and to the GRV, BK and DOLA models.*

One can notice the surprizing persistent rise of F_2 with decreasing x, even at very low Q^2, although this rise gets weaker with decreasing Q^2. Therefore the Donnachie-Landshoff model seems not to describe the data, even in the lowest Q^2 bin. The weakening of the rise of F_2 is however too strong in the model of GRV for the data below 1 GeV^2. The Badelek-Kwiecinski model [42] which combines a generalised Vector Meson Dominance approach at low Q^2 with a pQCD one at high Q^2 is able to reproduce the x-Q^2 behaviour of F_2 in this kinematic region.

The rise of F_2 as function of x can be quantified by fitting $F_2 \propto x^{-\lambda}$ at fixed Q^2 values for $x < 0.1$. The values of λ for such a fit on the 94 and the 95 data are displayed in fig. 10a. For $Q^2 \to 0$, λ approaches the value of 0.08 as expected in the photoproduction regime.

In fig. 10b, the effective virtual photon-proton cross-section is shown as function of Q^2 for different values of the invariant mass W, which is related to F_2 via:

$$\frac{d^2\sigma}{dxdQ^2} = \frac{2\pi\alpha^2}{xQ^4}\left[(2(1-y)+y^2)F_2(x,Q^2) - y^2F_L(x,Q^2)\right] \equiv \Gamma\sigma^{eff}_{\gamma^* p}(x,y,Q^2)$$

with $\Gamma = \alpha(2-2y+y^2)/2\pi Q^2 x$.

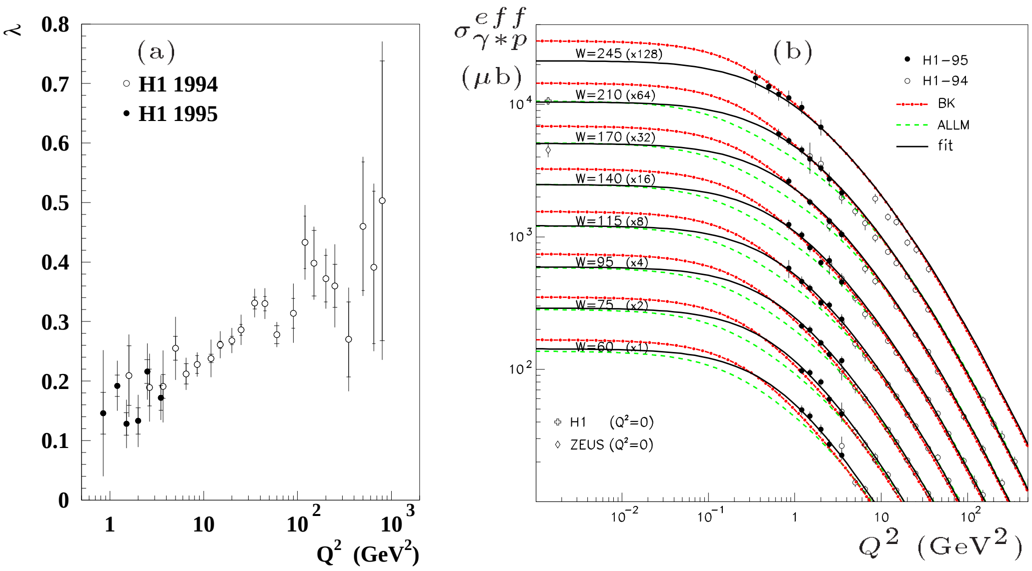

FIGURE 10. *a) The variation of the exponent λ expressing the slope of F_2 in x. b) Measuremens of the virtual photon-proton cross section $\sigma^{eff}_{\gamma * p}$ as function of Q^2.*

Both the BK model and the model of ALLM [43] fail to describe the data from $\simeq$ 0 GeV^2 to high Q^2. The model of ALLM gives a good limit for the measurement at $Q^2 = 0$ and at high Q^2, but tends to be too low in the transition region, whereas the BK model is too high at $Q^2 = 0$. Therefore a fit was performed following the BK approach with C$_{VDM}$ and Q_0^2 taken as free parameters, while they are equal to 1 and 0.8 GeV^2 in the original BK model.

$$F_2(x,Q^2) = C_{VMD}\cdot F_2^{\rm VMD}(x,Q^2) + \frac{Q^2}{Q_0^2+Q^2}F_2^{\rm QCD}(\overline{x},Q^2+Q_0^2)$$

The resulting fit shown in fig. 10 gives $C_{VMD} = 0.77$ and the unphysical value of $Q_0^2 = 0.45$GeV^2. Although it provides an overall good description of the data, the underlying dynamics has still to be understood.

VI CROSS-SECTIONS IN DIS AT HIGH Q^2

At High Q^2 the exchange of the W or the Z cannot be neglected anymore, and the differential cross-sections can be rewritten for the NC events as

$$\frac{\mathrm{d}^2\sigma^{\mathrm{NC}}(\mathrm{e}^{\pm}\mathrm{p})}{\mathrm{dxdQ}^2} = \frac{2\pi\alpha^2}{\mathrm{xQ}^4}\Big(\mathrm{Y}_+\mathcal{F}_2(\mathrm{x},\mathrm{Q}^2)\mp\mathrm{Y}_-\mathrm{x}\mathcal{F}_3(\mathrm{x},\mathrm{Q}^2)\Big) \quad ; \quad \mathrm{Y}_\pm \equiv (1\pm(1-\mathrm{y})^2)$$

The $\mathcal{F}_2$, $\mathcal{F}_3$ Structure functions of the proton include Z^o-propagator effects and ew-couplings: $\mathcal{F}_2$ contains the pure γ and Z^o exchange. $\mathcal{F}_3$ represent the $\gamma - Z^o$ interference term For the CC events the cross-sections can be expressed directly as a function of the quark densities ($q = q(x, Q^2)$, with $q = u, d, s, c$), G_μ being the Fermi–Coupling constant and M_W is the mass of the W boson in the propagator term.

$$\frac{d^2\sigma^{e^+p}}{dxdQ^2} = \frac{G_\mu^2}{\pi}\frac{M_W^2}{(M_W^2+Q^2)^2}((\bar{u}+\bar{c})+(1-y)^2(d+s))$$

$$\frac{d^2\sigma^{e^-p}}{dxdQ^2} = \frac{G_\mu^2}{\pi}\frac{M_W^2}{(M_W^2+Q^2)^2}((u+c)+(1-y)^2(\bar{d}+\bar{s}))$$

Two analyses are presented in the following. The first, based on 6 pb^{-1} of 1994-1995 data has been performed using the hadrons-only method, in order to compare with minimal systematic bias the NC and CC differential cross-sections [44]. The other using the full available statistics in H1 (14 pb^{-1} of 1994-1996 data) and an optimized reconstruction was oriented towards the study of very high Q^2 region [45].

• $d\sigma/dQ^2$ and $d\sigma/dx$ for NC and CC events
In the first analysis, the total Cross Section for Charged Current e^+p, was obtained with a a transverse momentum cut $p_t > 12.5GeV$ and a kinematic range restricted to $0.1 < y < 0.9$:

$$\sigma_{\mathrm{tot}}^{\mathrm{CC}} = (25.2 \pm 2.5 \pm 0.8)\mathrm{pb} \quad \text{preliminary)}$$

The differential cross-section $\frac{d\sigma}{dQ^2}$ (fig. 11a), $\frac{d\sigma}{dx}$ (fig. 11b) and $\frac{d\sigma}{dy}$ (cf [44]) show a good agreement with the standard model on the full kinematic range available with that statistics. The NC and CC cross-sections have comparable size for for $Q^2 \approx m_Z^2$ GeV^2. In future the y-differential CC cross section is expected to provide separate information on the valence and sea quark densities, due to the different y dependence of these two terms.

• The Very High Q^2 events
With the increase of luminosity, the capabilities of the detector, which was designed for the study of high Q^2 events, are fully exploited. Namely the H1

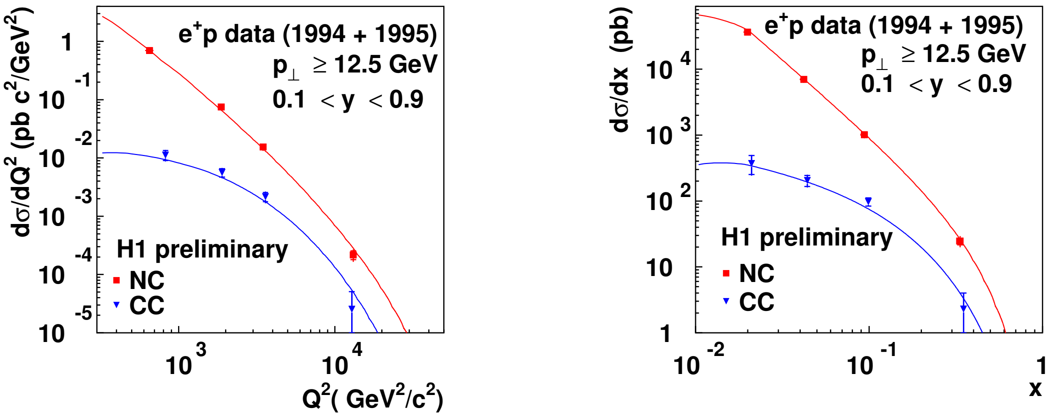

FIGURE 11. *NC and CC differential cross-section: a)* $d\sigma/dQ^2$ *; b)* $d\sigma/dx$ *.*

fine-grained Liquid Argon calorimeter ($\sim$ 44000 cells) allow the polar angle of the scattered electron to be measured with a 2 to 5 mrad accuracy, its energy with a resolution of $\sigma(E)/E \simeq 12\%/\sqrt{E/\mathrm{GeV}} \oplus 1\%$ and with an absolute scale known from test beams in most of the range studied of $\pm 3\%$.

The high Q^2 events are essentially background free due to their striking signature (see fig. 12). The predictions of the standard DIS model are precise (see [46] for a more detailed review) in this kinematic domain, since the electron probes the valence quarks at high x, which are constrained by the high statistics structure function fixed target experiments. The DGLAP evolution of these parton densities are also well understood at NLO, and the theoretical error on the cross-section prediction is below 10%, including the uncertainties on α_S, the shape of the "input" parton distributions, the evolution itself and the higher order QED corrections. These expectations have already been tested on the 1994 data in the high Q^2 F_2^p measurement at HERA, albeit with yet limited statistical precision, as can be seen in fig. 13.

The 1994-1996 analysis is performed at $Q^2 > 2500$ GeV^2 both on NC and CC. For the NC, the e method is used as a reference, while a complete cross-check has been done with the DA method. The main selection cuts are: $E_{T,e} > 25$GeV, $\Theta_e > 10^o$, $0.1 < y_e < 0.9$, plus additional conditions on the conservation of transverse and longitudinal momentum. The electron identification is done using "classic" estimators such as shower shape, isolation in $\eta - \phi$, and a loose track matching. The remaining background after these cuts is negligible. For the CC the main condition is the requirement of a missing momentum greater than 50 GeV.

The Q^2 distribution for NC events compared to the standard model histogram can be seen in fig 13a,b. An excess of events is visible above 15000 GeV^2, the 7 arrows pointing to the high y events discussed below. In CC

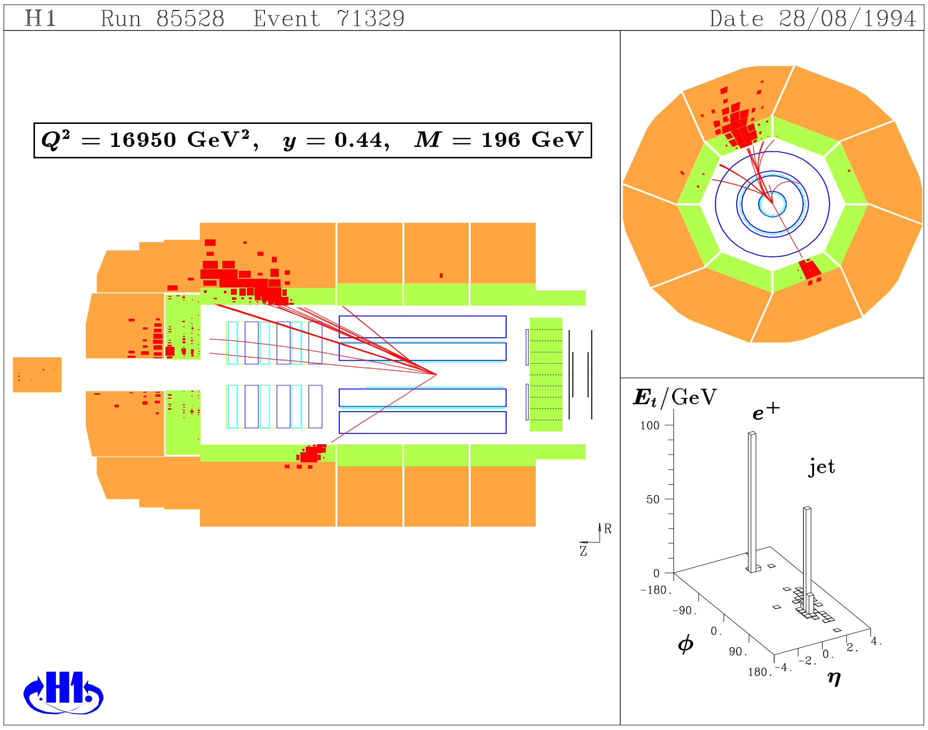

FIGURE 12. *One of the 7 high Q^2 high Mass NC events as visualized in the H1 detector with its fine-grained Liquid Argon calorimeter. The positron is on the bottom, the current jet on the upper part of the detector.*

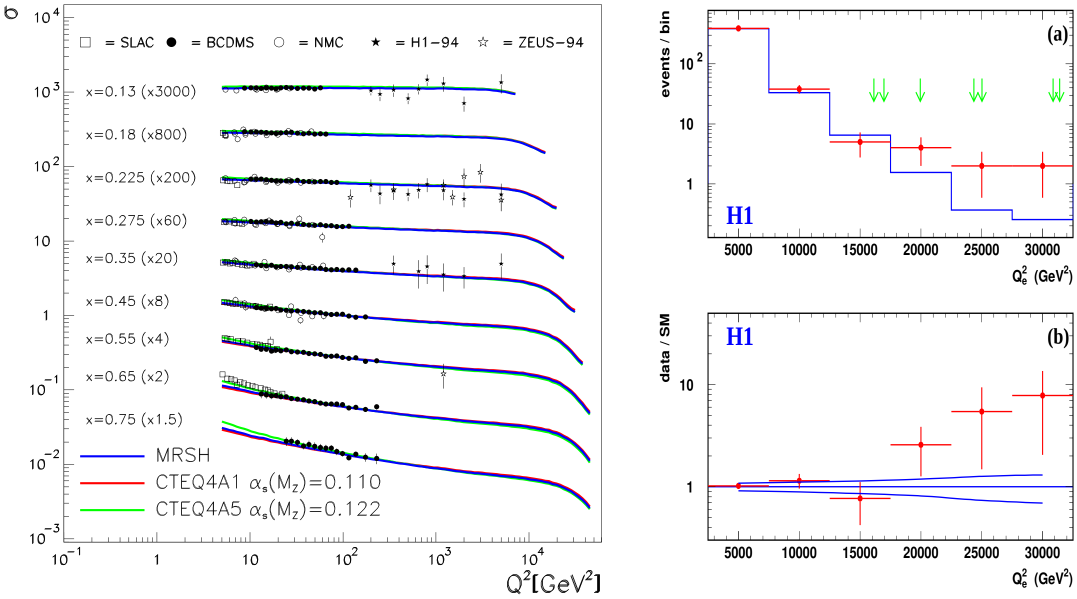

FIGURE 13. *Left: Double differential cross-section* $\frac{d^2\sigma^{NC}(e^{\pm}p)}{dxdQ^2}$ *as measured by DIS experiments and HERA in 1994. a) Raw Q^2 distribution for NC events displaying the excess above 15000 GeV^2. The arrows point to the 7 high mass, high y events (see text). b) ratio of data/standard model. The systematic error band is shown.*

events, no significant excess is observed (4 events detected for 1.77±0.87 expected). The significance of the excess seen in NC events is found in the following table which gives the probability of observing our number of events at $Q^2 > Q^2_{min}$.

Q^2_{min}(GeV^2)	2500	10000	15000	20000	30000
N_{obs}	443	20	12	5	2
N_{DIS}	426.7 ±38.4	18.3 ±2.4	4.71 ±0.76	1.32 ±0.27	0.23 ±0.05
$\mathcal{P}(N \geq N_{obs})$	0.35	0.39	6 10^{-3}	1.4 10^{-2}	2.3 10^{-2}

If applying a cut $y > 0.4$ in order to remove the largest part of the standard DIS expected events, 7 events at $Q^2 > 15000$ GeV^2 remain (see arrows in fig. 13a) and they are clustered at an invariant mass of 200 ±12.5 GeV, where only 0.95 ± 0.18 are expected. Several other methods have been used to derive the mass and all give the average result of 200 GeV (within 2 GeV) [45]. The Σ method has also been applied since it is independent of initial state QED radiation, and the results are given in table 2. The only event which might be radiative (event 5) as can be seen by comparing the kinematic variables reconstructed by the e, DA and Σ methods, is showing basically no change in its reconstructed mass.

evt	M_e (GeV)	M_Σ (GeV)	M_{DA} (GeV)	y_e	y_Σ	y_{DA}	Q^2_e (GeV^2)	Q^2_Σ (GeV^2)	Q^2_{DA} (GeV^2)
1	196	196	198	.439	.443	.434	16950	17100	17100
2	208	209	200	.563	.592	.582	24350	25930	23320
3	188	188	185	.566	.561	.573	19950	19760	19640
4	198	196	199	.790	.786	.787	30870	30230	31320
5	211	210	227	.562	.525	.526	25030	23120	27100
6	192	190	190	.440	.501	.443	16130	18140	16050
7	200	202	213	.783	.786	.762	31420	31940	34450

In conclusion the accumulation of these events at $M = 200$ GeV is genuine, but is not confirmed by the distribution of the ZEUS events at high Q^2 and high y. However ZEUS has also an excess of a few events in NC at very high Q^2. The systematic effects being well under control, both on the expectation side as on the detection side, more data are needed to understand if the observed excess at high Q^2 is due to a statistical fluctuations or to signs of new physics.

SUMMARY

A selected sample of H1 results presented at this workshop in the different areas of DIS has been summarized. The increase of the luminosity will bear significant improvements in all these fields, showing the potential of the HERA collider. Most awaited is an answer on the high Q^2 puzzle which might reveal signs of physics beyond the Standard Model.

ACKNOWLEDGMENTS

I would like to thank the organizers for an exciting and enjoyable workshop. Thanks also to the 15 H1 speakers of the parallel sessions who provided me with much of the material shown here and to John Dainton for a careful reading of the manuscript. Many thanks to Ursula Bassler for her great help both in the preparation of the talk and in the completion of the written report.

REFERENCES

1. H1 Collaboration, I. Abt et al., Nucl. Phys. **B407** (1993) 515.
2. ZEUS Collaboration, M. Derrick et al., Phys. Lett. **B316** (1993) 412.
3. ZEUS Collaboration, M. Derrick et al., Phys. Lett. **B315** (1993) 418.
4. H1 Collaboration, I. Abt et al., Nucl. Phys. **B429** (1994) 477.
5. H1 Collaboration, I. Abt et al., Phys. Lett. **B324** (1994) 241.
6. ZEUS Collaboration, M. Derrick et al., Phys. Rew. Lett. **75** (1995) 1006.
7. A. Mehta, Proceedings of the Diffractive Workshop in Eilat (1995).
8. J.P. Phillips, Proceedings of Int. Conf. on HEP'97 (pa02-061).
9. M. Glück, E. Reya, A.Vogt, Z. Phys **C53** (1992) 651.
10. A. Donnachie and P.V. Landshoff, Phys. Lett. **B348** (1995) 213.
11. M. Dirkmann, these proceedings.
12. C. Cormack, these proceedings.
13. B. List, these proceedings.
14. H. Jung, Comp. Phys. Comm. **86** (1995) 147.
15. H1 Collaboration, C. Adloff et al., DESY-97-098 (1997) *subm. to Phys. Lett. B*
16. K. Rabbertz, these proceedings.
17. Yu.L. Dokshitzer and B.R. Webber, Phys. Lett. **B352** (1995) 451.
18. G. Ingelman, Proceedings *Physics at HERA*, Hamburg (1991), eds W. Buchmüller and G. Ingelman, vol. 3., 1366.
19. S. Catani and M. Seymour, Nucl. Phys. B **485** (1997) 291.
20. DELPHI Collaboration, P. Abreu et al., Z. Phys. **C73** (1997) 229.
21. E. Mirkes and D. Zeppenfield, Phys. Lett. B **380** (1996) 205.
22. Yu. L. Dokshitzer, Sov. Phys. JETP **46** (1977) 641;
    V. N. Gribov and L.N. Lipatov, Sov. J. Nucl. Phys. **15** (1972) 438 and 675;
    G. Altarelli and G. Parisi, Nucl. Phys. **B126** (1977) 297.
23. E. A. Kuraev, L. N. Lipatov and V. S. Fadin, Sov. Phys. JETP **45** (1977) 19
    Y. Y. Balitsky and L.N. Lipatov, Sov. J. Nucl. Phys. **28** (1978) 822.
24. G. Marchesini et al., Comp. Phys. Comm. **67** (1992) 465.
25. L. Lönnblad, Comp. Phys. Comm. **71** (1992) 15.
26. M. Kuhlen, Phys. Lett. **382** (1996) 441.
27. H1 Collaboration, C. Adloff et al., Z. Phys. **C72** (1996) 573.
28. H1 Collab., T.Ahmed et al., Nucl. Phys. **B439** (1995) 471.
29. ZEUS Collab., M. Derrick et al., Z. Phys. **C65** (1995), 379.
30. H1 Collab., S. Aid et al., Nucl. Phys. **B470** (1996) 3.
31. ZEUS Collab., M.Derrick et al., Z. Phys. **C72** (1996) 399.

32. BCDMS Collab., A. C. Benvenuti et al., Phys. Lett. **B237** (1990)
33. NMC Collab., M. Arneodo et al., Phys. Lett. **B364** (1995) 107.
    NMC Collab., M. Arneodo et al., HEPPH-9610231 preprint, (1996).
34. H1 Collab., C. Adloff et al., Phys. Lett. **393B** (1997) 452.
35. H1 Collab., C.Adloff et al., DESY 97-042 (1997) *subm. to Nucl. Phys. B.*
36. L. Whitlow et al., Phys. Lett. **B250** (1990) 93.
37. NMC Collaboration, M. Arneodo et al, hep-ph/9610231, *subm. to Nucl. Phys.*
38. G. Altarelli and G. Martinelli, Phys. Lett. **B76** (1978) 89.
39. M. Glück, E. Reya and A. Vogt, Z. Phys **C67** (1995) 433; A. Vogt, Proceedings of the Workshop on Deep-Inelastic Scattering and QCD, Paris (1995) 261, using the NLO charm contribution as calculated in [40].
40. E.Laenen et al., Nucl. Phys. **B392** (1993) 162, ibid. (1993) 229;
    E.Laenen et al., Phys. Lett. **B291** (1992) 325;
    S.Riemersma et al., Phys. Lett. **B347** (1995) 143.
41. A. Donnachie and P.V. Landshoff, Z. Phys. **C61** (1994) 139.
42. B. Badelek, J. Kwiecinski and A. Stasto, Durham preprint DTP/96/16 (1996).
43. H. Abramowicz, E.M. Levin, A. Levy and U. Maor, Phys. Lett. **B269** (1991) 466; A. Marcus PhD. thesis Tel-Aviv University TAUP 2350-96 (1996).
44. S. Riess, these proceedings.
45. H1 Collab., C.Adloff et al., Z. Phys C74 (1997) 191.
46. R. G. Roberts, these proceedings.